

Multi-band optical variability studies of BL Lacertae

Aditi Agarwal^{1,2*} and Alok C. Gupta^{1,2}

¹Aryabhata Research Institute of Observational Sciences (ARIES), Manora Peak, Nainital – 263002, India

²Department of Physics, DDU Gorakhpur University, Gorakhpur - 273009, India

Accepted Received; in original form

ABSTRACT

We monitored BL Lacertae for 13 nights in optical B, V, R, and I bands during October and November 2014 including quasi-simultaneous observations in V and R bands using two optical telescopes in India. We have studied multi-band optical flux variations, colour variation and spectral changes in this blazar. Source was found to be active during the whole monitoring period and showed significant intraday variability on 3 nights in V and R filters while displayed hints of variability on 6 other dates in R passband and on 2 nights in V filter. From the colour-magnitude analysis of the source we found that the spectra of the target gets flatter as it becomes brighter on intra-night timescale. Using discrete correlation technique, we found that intraday light curves in both V and R filters are almost consistent and well correlated with each other. We also generated spectral energy distribution (SED) of the target using the B, V, R, and I data sets for all 13 nights which could help us investigate the physical process responsible for the observed variations in BL Lacertae objects. We also discuss possible physical causes of the observed spectral variability.

Key words: BL Lacertae objects: general — : galaxies — active — quasars: individual – BL Lacertae

1 INTRODUCTION

BL Lacertae objects and high polarization sources called as flat spectrum radio quasars (FSRQs) together constitute a violently variable class of Active Galactic Nuclei (AGNs) known as blazars (e.g., Blandford & Rees 1978, Ghisellini et al. 1997). Common blazar characteristics include high polarization, synchrotron emission from the relativistic jet, rapid flux variability, core-dominated radio morphology, flat radio spectrum and many more owing to the relativistic motion of plasma in the jets extending on even Mpc scales, pointing at angles $\leq 10^\circ$ with the line of sight (LOS) thus causing the observed emission to be relativistically beamed (e.g., Urry & Padovani 1995). Blazars are known to be variable at all accessible time scales over entire electro-magnetic spectra. Magnitude changes of few hundredth to tenths over a time scale of a day is called intraday variability (IDV) or micro-variability (Wagner & Witzel 1995, Rector & Perlman 2003) which help us in probing innermost regions of AGNs; changes from several days to few months are usually known as short time variability (STV); while those taking from several months to many years are usually called long term variability (LTV; Gupta et al. 2004), in last two classes blazar variability can usually exceed even ~ 5 mag.

Flux variability usually leads to spectral changes due to the changes in the spectra of emitting electrons along with the activity associated with the relativistic Doppler boosted jets. The

spectral energy distribution (SED) of blazars display two well-defined broad spectral components (Mukherjee et al. 1997; Weekes 2003). Based on the location of these peaks, we have low energy peaked blazars (LBLs) whose first component peaks in near-IR (NIR)/optical while the second component usually peaks at GeV energies and high energy peaked blazars (HBLs) where first peak is in UV/X-rays while the second peak at TeV energies (Padovani & Giommi 1995, Abdo et al. 2010). During flaring state the peak is found to be shifted towards higher frequencies. Spectral properties were linked with the source luminosity by Fossati et al. (1997) such that HBLs were the low luminosity objects with high space density and high electron density thus high magnetic field while the objects with high luminosity, low space density plus low magnetic field were named LBLs. Ratio of X-ray flux in the 0.3-3.5 keV band to the radio flux density at 5GHz is also used to classify as low-synchrotron-peaked or high-synchrotron-peaked blazars (LSPs or HSPs) based on whether the ratio is smaller or greater than $10^{-11.5}$ respectively (Padovani & Giommi 1996). In addition to LSPs and HSPs we also have intermediate synchrotron peaked blazars (ISPs) also for which SED peaks are located at intermediate frequencies (Sambruna, Maraschi & Urry 1996). One can also define LSPs as those blazars with energy peak frequency of their synchrotron hump, $\nu_{\text{peak}} \sim 10^{13-14}$ Hz, ISPs as those with $\nu_{\text{peak}} \sim 10^{15-16}$ Hz while those with $\nu_{\text{peak}} \sim 10^{17-18}$ Hz as HSPs. The above classification was proposed by Nieppola, Tornikoski & Valtaoja (2006) based on the studies of 300 BL Lacertae objects. From the observational point of view it has been found that LBLs

* E-mail: aditi@aries.res.in

are more optically variable than HBLs (Stocke et al. 1985; 1989; Heidt & Wagner 1996)

BL Lacertae ($\alpha_{2000.0} = 22^{\text{h}} 02^{\text{m}} 43.29^{\text{s}}$ $\delta_{2000.0} = +42^{\circ} 16' 39.98''$) located at a redshift value of $z = 0.069$ (Miller & Hawley 1977) with a moderately bright elliptical host galaxy (Wurtz, Stocke & Yee 1996), is a prototype of the blazar class of AGNs which has been intensively studied since its discovery by Schmitt (1968) with radio source VRO 42.22.01 and characterized by a featureless spectrum. BL Lacertae is classified as a low-frequency peaked blazar (Fossati et al. 1998; Abdo et al. 2010) with first component of its SED peaking in near-IR (NIR)/optical region which can be explained by synchrotron emission from the helical jet (Raiteri et al. 2009), thus making optical studies of the BL Lacertae helpful to understand them in greater detail. Optical observations can also indicate the possible presence of other components in addition to synchrotron continuum. There is good evidence for the presence of IDV and colour variability in some BL Lacertae objects and our source is among those (e.g., Carini et al. 1992, Clements & Carini 2001, Gu et al. 2006, H.E.S.S. Collaboration et al. 2011). Due to its pronounced variability over entire electromagnetic spectra it has been continuously monitored with Whole Earth Blazar Telescope (WEBT)¹ since 1997 till today; which involves four major WEBT multi-frequency campaigns, two of them were organized in 1999 supplemented with ASCA and Beppo SAX observations (Ravasio et al. 2002) while the other two provided densely sampled, high precision, long term campaigns carried out during May 2000 - January 2001 and May 2001 - February 2002 (Villata et al. 2002; Böttcher et al. 2003; Villata et al. 2004a,b).

Carini et al. (1992) studied two optically bright sources, OJ 287 and BL Lacertae using a decade long photometric observations where they found IDV of the order of 0.08 mag/hr in former and 0.01 mag/hr for later. Authors also detected hints of bluer-when-brighter (BWB) trend but any relation between spectral and flux changes were absent. Later, Villata et al. (2002, 2004a) confirmed the presence of BWB trend in short isolated outburst but not on long timescales for BL Lacertae, indicating two different components are operating. Heidt & Wagner (1996) found 80% of complete BL Lacertae objects to show IDV confirming it to be their intrinsic nature. During the 1997 optical outburst of our target, strong correlation was found between V-R colour and R magnitude with the correlation coefficient reaching ~ 0.7 in 11 nights. Although blazar colour variability has been extensively studied since many years, but is still a hot topic of discussion, particularly for BL Lacertae, where underlying bright elliptical galaxy contaminating the photometric magnitudes mainly at low flux levels, could be one of the reasons. Rise and decay timescales for the target have also been studied by Papadakis et al. (2003) and found them increasing with frequency. Significant flux-flux correlation (Raiteri et al. 2013) has been established from extensive optical studies of the BL Lacertae objects.

In this paper, our aim is to have a flavor of variability nature of the source BL Lacertae on shortest possible timescale; study colour and spectral change; and to have an idea about the process occurring in the vicinity of the central super massive black hole (SMBH) through photometric studies of flux variations.

The structure of the paper is as follows: In Section 2, we present the details of the observations and data reduction procedures. Section 3 describes various analysis techniques used, while the variability results are reported in Section 4, followed by corre-

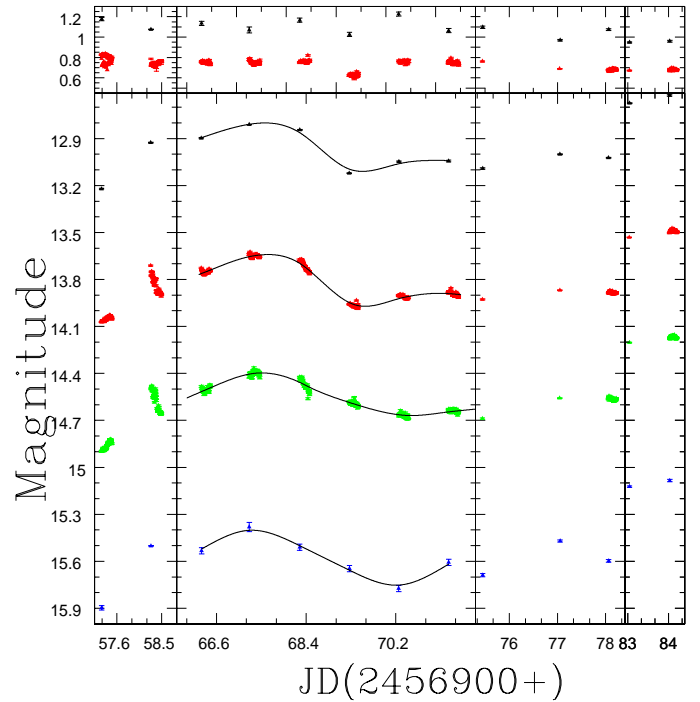


Figure 1. Light curves for BL Lacertae covering full monitoring period; blue denotes B filter; green denotes V filter; red, R filter; and black, I filter. Y axis is the magnitude while x-axis is Julian Date (JD). In the top panel red colour represents (V-R) colour variation while black is for (B-I) — 1.7 colour. Offset of 1.7 is used with (B-I) plot to avoid its eclipsing with (V-R) plot. Solid line represents a cubic spline interpolation during the continuous 6 nights monitoring in B, V, R, and I filters.

lation studies in Section 5 and colour variability studies in Section 6. Section 7 describes the spectral changes in the source and finally discussion and conclusion are given in Section 8.

2 OBSERVATIONS AND DATA REDUCTIONS

Observations of the BL Lacertae were carried out using two optical telescopes of India, one is the 1.04 m Sampuranand telescope with f/13 Cassegrain focus located at Aryabhata Research Institute of observational sciencES (ARIES), Nainital and the other one is the 1.3-m Devasthal fast optical telescope (DFOT) of ARIES, Nainital, India. Both these telescopes are equipped with CCD detectors and broadband Johnson UBV and Cousins RI filters. Technical parameters and instrumental details are summarized in Table 1. The optical photometric data for BL Lacertae was gathered between 25 Oct to 23 Nov 2014. For the pre-processing of the raw data we used standard procedures in the IRAF² software following the steps described below. Bias frames were taken at regular intervals covering whole night which are used to generate a master bias for that particular observation night by taking median of all bias frames. This master bias was subtracted from all twilight flat frames and the image frames. Next step in the initial processing is of flat fielding

¹ <http://www.oato.inaf.it/blazars/webt/>

² IRAF is distributed by the National Optical Astronomy Observatories, which are operated by the Association of Universities for Research in Astronomy, Inc., under cooperative agreement with the National Science Foundation.

Table 1:

A: 1.04 m telescope, ARIES, Nainital, India
 B: 1.3 m Ritchey-Chretien Cassegrain optical
 telescope, ARIES, Nainital, India

Site:	A	B
Telescope:	1.04-m RC Cassegrain	1.30m Ritchey-Chretien
CCD model:	Wright 2K CCD	Andor 2K CCD
Chip size:	2048 × 2048 pixels	2048 × 2048 pixels
Pixel size:	24 × 24 μm	13.5 × 13.5 μm
Scale:	0.37''/pixel	0.535''/pixel
Field:	13' × 13'	18' × 18'
Gain:	10 e^- /ADU	1.4 e^- /ADU
Read Out Noise:	5.3 e^- rms	4.1 e^- rms
Binning used:	2 × 2	2 × 2
Typical seeing :	1'' to 2.8''	1.2'' to 2.0''

Table 2

Date of observations (yyyy mm dd)	Telescope	Number of data points Filters (B,V,R,I)
2014 10 26	A	1,42,42,1
2014 10 27	A	1,42,43,1
2014 11 04	A	1,31,31,1
2014 11 05	A	1,44,44,1
2014 11 06	A	1,42,42,1
2014 11 07	A	1,35,35,1
2014 11 08	A	1,45,45,1
2014 11 09	A	1,49,49,1
2014 11 13	A	1,1,1,1
2014 11 15	B	1,1,1,1
2014 11 16	B	1,46,46,1
2014 11 21	B	1,1,1,1
2014 11 22	B	1,52,52,1

Table 1. Details of telescopes and instruments

Table 2. Observation log of photometric observations of BL Lacertae

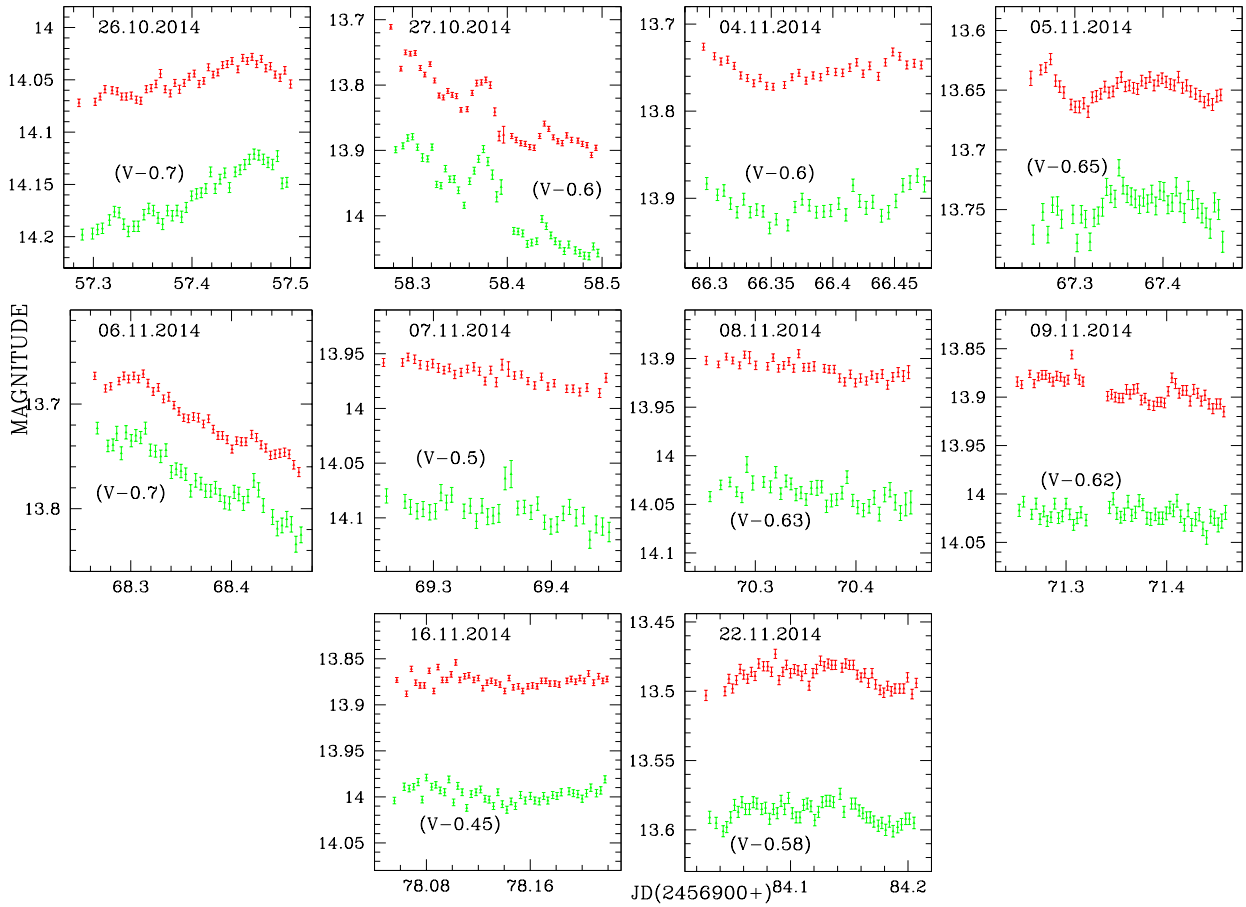


Figure 2. Light curves for BL Lacertae; green denotes V filter; red, R filter. Y axis is the magnitude in each plot while X axis is JD. Observation date is indicated in each plot.

Table 3. Results of IDV observations of BL Lacertae. Column 1 is the date of observation, column 2 indicates the band in which observations were taken, column 3 represents number of data points in a particular band, in the next three columns i.e. 4, 5, and 6 we have listed the results for C-statistic, F-test and χ^2 -test, respectively, followed by variability status in column 7 and finally the intra-night variability amplitude is given in column 8.

Date	Band	N	C_1, C_2, C_{avg}	F-test	χ^2 test	Variable	A%
				$F_1, F_2, F, F_c(0.99), F_c(0.999)$	$\chi^2_1, \chi^2_2, \chi^2_{av}, \chi^2_{0.99}, \chi^2_{0.999}$		
26.10.2014	V	42	3.5587, 3.0478, 3.3033	12.67, 9.29, 10.98, 2.09, 2.69	328.66, 238.62, 283.64, 65.95, 74.75	Var	7.67
	R	42	2.8122, 2.8627, 2.8375	7.90, 8.19, 8.05, 2.09, 2.69	248.54, 249.99, 249.26, 65.95, 74.75	Var	4.37
	(V-R)	42	2.1598, 1.6191, 1.8894	4.66, 2.62, 3.64, 2.09, 2.69	125.14, 69.93, 97.53, 65.95, 74.75	PV	6.24
27.10.2014	V	40	3.3657, 3.9467, 3.6562	11.33, 15.58, 13.45, 2.13, 2.76	400.44, 504.13, 452.28, 62.43, 72.05	Var	22.79
	R	40	9.2009, 9.1329, 9.1669	84.66, 83.41, 84.03, 2.13, 2.76	3006.4, 2791.2, 2898.8, 62.43, 72.05	Var	15.69
	(V-R)	40	1.9050, 1.3330, 1.6190	3.63, 1.78, 2.70, 2.13, 2.76	124.42, 133.04, 128.73, 62.43, 72.05	PV	6.94
04.11.2014	V	31	1.5193, 1.7475, 1.6334	2.31, 3.05, 2.68, 2.39, 3.22	151.19, 161.24, 156.21, 50.89, 59.70	PV	5.92
	R	31	2.2875, 2.3634, 2.3254	5.23, 5.58, 5.41, 2.39, 3.22	140.91, 85.86, 113.38, 50.89, 59.70	PV	4.56
	(V-R)	31	0.7035, 1.0318, 0.8676	0.50, 1.06, 0.78, 2.39, 3.22	9.47, 12.96, 11.21, 50.89, 59.70	NV	–
05.11.2014	V	43	1.5208, 1.5623, 1.5416	2.31, 2.44, 2.38, 2.38, 2.66	68.56, 49.08, 58.82, 66.21, 76.08	PV	6.21
	R	43	2.1314, 2.0030, 2.0672	4.54, 4.01, 4.28, 2.38, 2.66	203.64, 156.18, 179.91, 66.21, 76.08	PV	4.35
	(V-R)	43	1.5656, 1.5073, 1.5364	2.45, 2.27, 2.36, 2.38, 2.66	86.54, 58.20, 72.37, 66.21, 76.08	NV	–
06.11.2014	V	41	5.4723, 5.1830, 5.3276	29.95, 26.86, 28.40, 2.09, 2.69	776.44, 463.29, 619.86, 64.95, 74.74	Var	11.06
	R	41	6.8721, 6.8382, 6.8552	47.22, 46.76, 46.99, 2.09, 2.69	1804.10, 1692.90, 1748.50, 64.95, 74.74	Var	9.38
	(V-R)	41	1.2996, 1.2186, 1.2591	1.69, 1.48, 1.59, 2.09, 2.69	51.70, 32.09, 41.89, 64.95, 74.74	NV	–
07.11.2014	V	34	1.2005, 0.9753, 1.0879	1.44, 0.95, 1.20, 2.29, 3.04	13.55, 12.25, 12.9, 54.77, 63.87	NV	–
	R	35	2.0896, 2.1564, 2.1230	4.37, 4.65, 4.51, 2.26, 2.98	65.64, 104.59, 85.11, 56.06, 65.25	PV	5.17
	(V-R)	32	1.2802, 0.9024, 1.0912	1.64, 0.81, 1.23, 2.35, 3.15	17.34, 11.42, 14.38, 52.19, 61.09	NV	–
08.11.2014	V	36	1.5381, 1.5667, 1.5524	2.37, 2.45, 2.41, 2.23, 2.93	46.53, 31.72, 39.12, 57.34, 66.62	NV	–
	R	35	1.5678, 1.8589, 1.7134	2.46, 3.45, 2.96, 2.26, 2.98	71.42, 96.85, 84.13, 56.06, 65.25	PV	3.14
	(V-R)	35	1.1850, 1.1754, 1.1802	1.40, 1.38, 1.39, 2.26, 2.98	31.86, 23.91, 27.88, 56.06, 65.25	NV	–
09.11.2014	V	49	0.9388, 1.0879, 1.0134	0.88, 1.18, 1.03, 1.98, 2.49	24.12, 22.76, 23.44, 73.68, 84.04	NV	–
	R	49	1.5703, 2.0319, 1.8011	2.47, 4.13, 3.30, 1.98, 2.49	91.42, 100.00, 95.71, 73.68, 84.04	PV	5.86
	(V-R)	48	0.9525, 1.4293, 1.1909	0.91, 2.04, 1.47, 1.99, 2.51	27.96, 44.81, 36.38, 72.44, 82.72	NV	–
16.11.2014	V	46	1.0017, 0.8398, 0.9207	1.00, 0.70, 0.85, 2.02, 2.57	41.30, 75.73, 58.51, 69.96, 80.08	NV	–
	R	46	1.2413, 1.1424, 1.1919	1.54, 1.30, 1.42, 2.02, 2.57	35.02, 45.83, 40.42, 69.96, 80.08	NV	–
	(V-R)	46	0.9653, 0.6830, 0.8242	0.93, 0.47, 0.70, 2.02, 2.57	38.53, 50.76, 44.64, 69.96, 80.08	NV	–
22.11.2014	V	51	1.1749, 0.9398, 1.0573	1.38, 0.88, 1.13, 1.95, 2.44	69.79, 50.85, 60.32, 76.15, 86.66	NV	–
	R	51	1.6082, 1.3373, 1.4728	2.59, 1.79, 2.19, 1.95, 2.44	134.92, 95.32, 115.12, 76.15, 86.66	PV	2.96
	(V-R)	51	1.1525, 0.8490, 1.0007	1.33, 0.72, 1.02, 1.95, 2.44	66.15, 40.32, 53.23, 76.15, 86.66	NV	–

Var : Variable, PV : probable variable, NV : Non-Variable

when master flat in each filter is generated by median combine of all the flat frames in a particular passband. Next, normalized master flat for each passband is generated by which each source image frame was divided to remove pixel to pixel inhomogeneities. Finally, cosmic ray removal was carried out for all source image frames. Data processing was then done using the Dominion Astronomical Observatory Photometry (DAOPHOT II) software (Stetson 1987; Stetson 1992) to get the instrumental magnitudes of the BL Lac and the comparison stars by performing the concentric circular aperture photometry technique. For every night, we carried out aperture photometry with four different aperture radii, i.e., $\sim 1 \times \text{FWHM}$, $2 \times \text{FWHM}$, $3 \times \text{FWHM}$ and $4 \times \text{FWHM}$, out of which aperture radii of $2 \times \text{FWHM}$ was finally selected for our analysis as it provided the best S/N ratio. We observed more than three local standard stars on the same field. Out of these, we used those two comparison stars which had magnitude and colour similar to that of the blazar to avoid any error occurring from differences in the photon statistics in the differential photometry of the source. Comparison stars used for differential photometry of the blazar are stars B and C of the finding chart from the webpage³. Since the BL Lacertae and the standard stars magnitudes were obtained simultaneously under

same air mass and weather conditions, so the flux values are considered reliable. To get the calibrated magnitude of the target, that non variable standard star was chosen which had colour closest to the BL Lacertae.

We used MATLAB software to write additional programs for data processing. We observed BL Lacertae on continuous 6 nights from 4 Nov to 9 Nov 2014 quasi-simultaneously in V and R bands to study the IDV characteristics of the object and also to search for any possible time lags between these bands. We took single data points in B and I bands also and found that the source showed substantial brightness changes in all optical bands.

B, V, R and I light curves (LCs) of the BL Lacertae during our full monitoring period are displayed in Figure 1 where we fitted smoothing splines (Bachev et al. 2011) on the light curve (LC) during continuous monitoring period between 4 Nov to 9 Nov, which helps us to reveal the variability characteristics and time lags more clearly. The upper panel of the Figure 1 represent (B-I) and (V-R) variations with time.

The observation log is given in Table 2 where we have listed observation date, telescope used and number of data points for each date in a particular filter. The source shows clear evidence of IDV on 3 nights in both V band and R band.

³ <http://www.lsw.uni-heidelberg.de/projects/extragalactic/charts/2200+420.html>

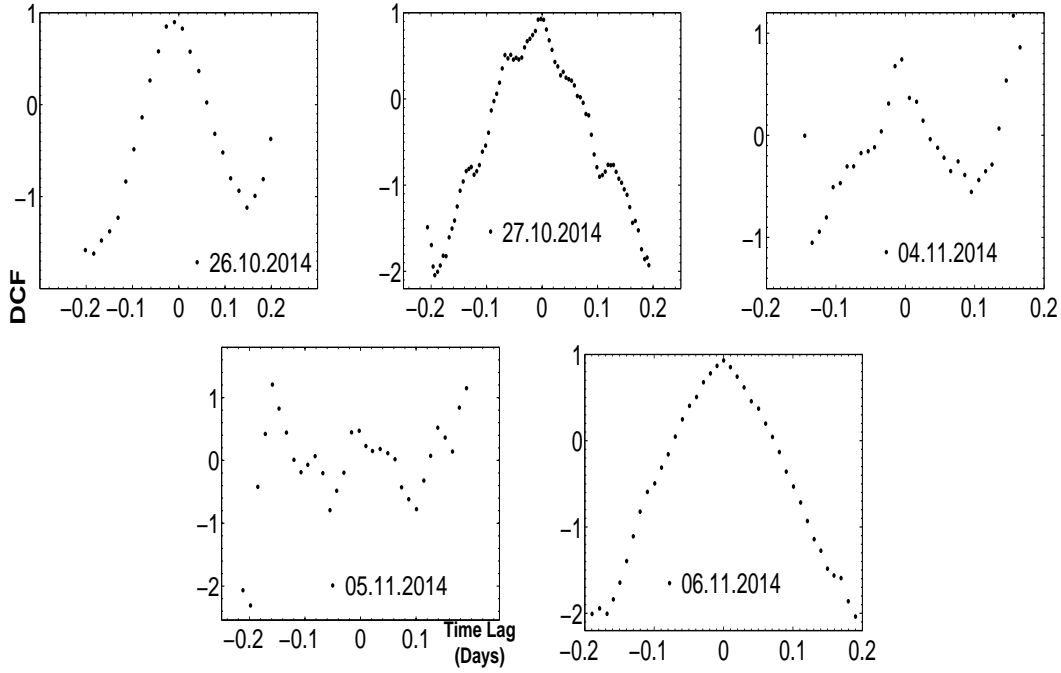


Figure 3. DCF plots between V and R passbands on intraday timescales for those nights when variability was detected in both the bands. The DCF values are given on the Y-axis and the Time Lag is plotted against them for each labeled date of observation.

3 ANALYSIS TECHNIQUES

To investigate variability properties of BL Lacertae we used a series of statistical analysis techniques to state that the extracted results are statistically significant. All these statistical tools are developed using MATLAB.

3.1 Variability detection criterion

To quantify the intraday variability nature of the source we have employed three different statistics (e.g., de Diego 2010) named as C test, F test and χ^2 test.

3.1.1 C-Test

To claim the variability of the source we used the most frequently used criterion introduced by Romero, Cellone, & Combi (1999), where the variability detection parameter C_{avg} is defined as the average of C_1 and C_2 with:

$$C_1 = \frac{\sigma(BL - StarA)}{\sigma(StarA - StarB)}, \quad C_2 = \frac{\sigma(BL - StarB)}{\sigma(StarA - StarB)}. \quad (1)$$

Here (BL–Star A), (BL–Star B), and (Star A–Star B) are the differential instrumental magnitudes of the blazar and standard star A, the blazar and standard star B, and standard star A vs. standard star B determined using aperture photometry of the source and comparison stars, whereas $\sigma(BL - starA)$, $\sigma(BL - starB)$ and $\sigma(Star A - Star B)$ are observational scatters of the differential instrumental magnitudes of the blazar–Star A, blazar–Star B, and Star A–Star B, respectively, with star A and star B being those two stars having $\sigma(Star A - Star B)$ to be minimum. According to the adopted variability criterion, if $C_{avg} \geq 2.57$, then the nominal confidence level of variability detection is $> 99\%$ (Jang & Miller 1997; Stalin et al. 2004; Gupta et al. 2008). If observations are done in three or

more than three filters then C_{avg} value should be ≥ 2.576 in at least two filters for the source to be reported variable.

3.1.2 F-Test

de Diego (2010) mentioned the C-test to be too conservative in quantifying variability. F test is considered to be a proper statistics to test any changes of variability. F values compare two sample variances and are calculated as:

$$F_1 = \frac{Var(BL - StarA)}{Var(BL - StarB)}, \quad F_2 = \frac{Var(BL - StarA)}{Var(StarA - StarB)}. \quad (2)$$

Here (BL–Star A), (BL–Star B), and (Star A–Star B) are the differential instrumental magnitudes of blazar and star A, blazar and star B, and star A and star B, respectively, while $Var(BL - Star A)$, $Var(BL - Star B)$, and $Var(Star A - Star B)$ are the variances of differential instrumental magnitudes.

We take the average of F_1 and F_2 to find a mean observational F value. The F value is then compared with $F_{\nu_{bl}, \nu_*}^{(\alpha)}$, a critical value, where ν_{bl} and ν_* respectively denote the number of degrees of freedom for the blazar and star, while α is the significance level set as 0.1 and 1 percent (i.e 3σ and 2.6σ) for our analysis. If the mean F value is larger than the critical value, the null hypothesis (i.e., that of no variability) is discarded. Nightly LCs and colour indices are listed as variable if $F > F_c(0.99)$.

3.1.3 χ^2 -test

To investigate the presence of IDV we also performed a χ^2 -test. The χ^2 statistic is defined as

$$\chi^2 = \sum_{i=1}^N \frac{(V_i - \bar{V})^2}{\sigma_i^2}, \quad (3)$$

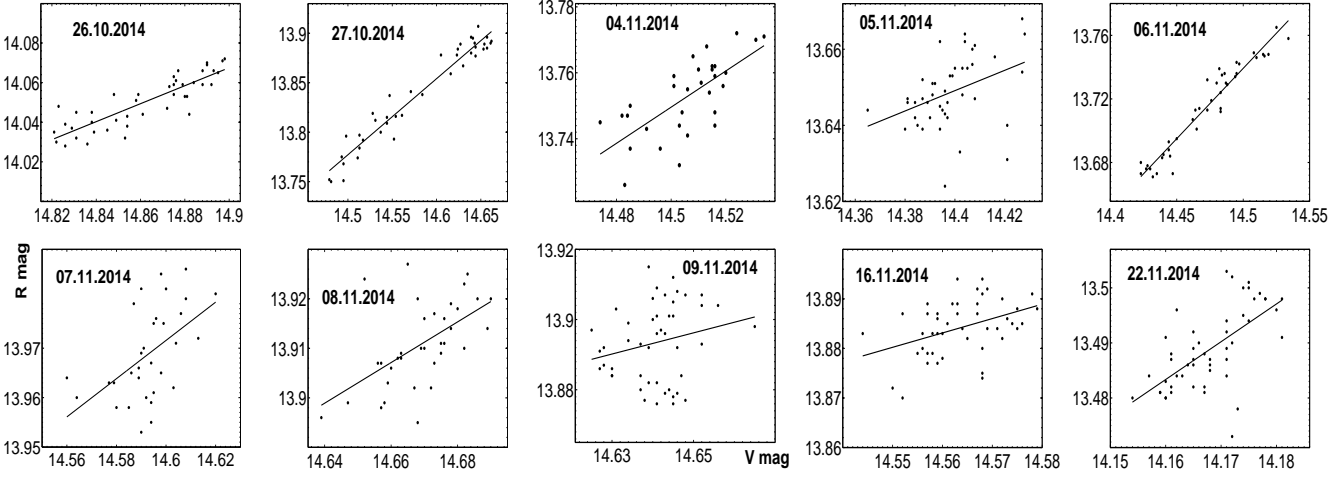


Figure 4. R magnitude (y-axis) Vs V magnitude (x-axis) plots on intra-night timescale for 10 observation days.

where, \bar{V} is the mean magnitude, and the i th observation yields a magnitude V_i with a corresponding standard error σ_i which is due to photon noise from the source and sky, CCD read-out and other non-systematic error sources. Exact quantification of such errors by the IRAF reduction package is impractical and it has been found that theoretical errors are smaller than the real errors by a factor of 1.3–1.75 (e.g., Gopal-Krishna et al. 2003, Gupta et al. 2008) which for our data is ~ 1.5 , on average. So the errors obtained after data reduction should be multiplied by this factor to get better estimates of the real photometric errors. This statistic is then compared with a critical value $\chi^2_{\alpha, \nu}$ where α is again the significance level set same as in case of F test while $\nu = N - 1$ is the degree of freedom. $\chi^2 > \chi^2_{\alpha, \nu}$ implies the presence of variability.

3.1.4 Percentage amplitude variation

The percentage variation on a given night is calculated by using the variability amplitude parameter A , introduced by Heidt & Wagner (1996), and defined as

$$A = 100 \times \sqrt{(A_{max} - A_{min})^2 - 2\sigma^2}(\%), \quad (4)$$

where A_{max} and A_{min} are the maximum and minimum values in the calibrated LCs of the blazar, and σ is the average measurement error.

3.2 Discrete correlation function (DCF)

To search for and quantify any possible correlations between the optical fluxes we used the DCF technique. The DCF method was first introduced by Edelson & Krolik (1988). For details on DCF see Hovatta et al. (2007); Rani, Wiita, & Gupta (2009), and references therein.

The DCF method is defined as: for each pair of data (x_i, y_j) , with $0 \leq i, j \leq N$, with N the number of data points, the unbinned discrete correlation function (UDCF) is

$$UDCF_{ij}(\tau) = \frac{(x_i - \bar{x})(y_j - \bar{y})}{\sqrt{(\sigma_x^2 - e_{x^2})(\sigma_y^2 - e_{y^2})}} \quad (5)$$

where the parameters \bar{x}, \bar{y} are the mean values of the two discrete data series x_i, y_j , with standard deviations σ_x, σ_y and measurement errors e_x, e_y .

The DCF can be calculated by averaging the UDCF values (M in number) for each time delay $\Delta t_{ij} = (t_{yj} - t_{xi})$ lying in the range $\tau - \frac{\Delta\tau}{2} \leq t_{ij} \leq \tau + \frac{\Delta\tau}{2}$ and is expressed as

$$DCF(\tau) = \frac{\sum_{k=1}^M UDCF_k}{M}, \quad (6)$$

where τ is the center of the bin of size $\Delta\tau$. The error is found from the standard deviations of the number of bins used for determining the DCF and is given as:

$$\sigma_{DCF(\tau)} = \frac{\sqrt{\sum_{k=1}^M (UDCF_k - DCF(\tau))^2}}{M - 1}. \quad (7)$$

When correlating a data series with itself ($x = y$), we obtain the auto-correlation function (ACF) with a peak at $\tau = 0$, indicating the absence of any time lag while any other strong peak indicates the presence of periodicity. In general, a DCF value > 0 implies the two data signals are correlated, while the two anti-correlated data sets have a DCF < 0 , and a DCF value equal to 0 implies no correlation exists between the two data trains. Additional advantage of this method is that it is suitable for unevenly sampled data as is the case in most astronomical observations.

4 FLUX AND COLOUR VARIABILITY RESULTS

We observed the blazar BL Lacertae on 13 nights in B, V, R, and I passbands which includes quasi-simultaneous observations in V and R passbands on 10 of these 13 nights. The complete observation log for this blazar is given in Table 2. Intra-night LCs in V and R filters taken quasi-simultaneously are plotted in Figure 2. We applied C-statistics, F-test and χ^2 -test, as discussed above. Our analysis results on intranight timescales for V and R filters are summarized in Table 3. The blazar is marked as variable (Var) if the variability conditions for each test mentioned under Section 3.1 are satisfied, while its marked probably variable (PV) if conditions for either of the two tests are followed, and finally the quasar is marked Non-variable (NV) if none of the conditions are met by the target. The source was found to be in active state during our entire span of observations with clear variability found on 3 nights as evident from the Table 3 on 26 Oct, 27 Oct and 6 Nov 2014 in both V and R bands. There was a prominent variation on 27 October 2014 around

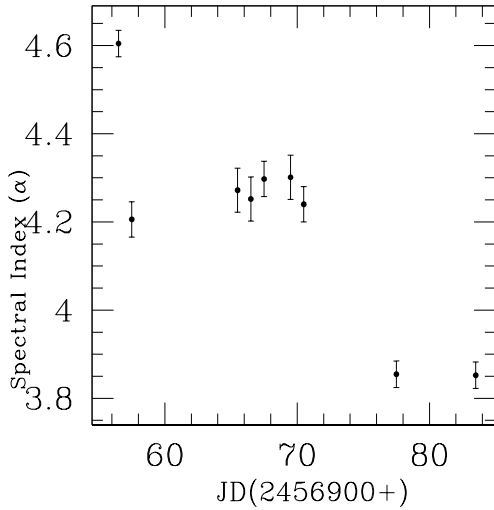


Figure 5. Variation of average optical spectral index calculated using equation 8 Vs time covering the entire observation period for the BL Lacertae.

JD 245658.35 with amplitude of about ~ 0.05 mag followed by another short flaring event around JD 245658.43 of ~ 0.04 mag in R passband. Similar trend was found in V passband as shown in Figure 2 from which it is evident that the data sets for these events in both the bands are consistent with each other. The object reached the faintest level of 14.07 mag in R passband which is still ~ 1 mag brighter than its historical maximum magnitude as reported by Fan & Lin (2000). While on the last day of our observation span i.e., on 22 November, source was found to be the brightest with a magnitude of 15.08, 14.15, 13.4, and 1.624 in B, V, R, and I passbands, respectively, indicating that the source might go into flaring state in near future. The intra-night variability amplitude was minimum on 22 Nov with value 2.96% in R filter while reached maximum value of 18.28% on 27 Oct in V passband when source showed ~ 0.18 mag change in 3.5 hours of observation duration in V passband. As can be seen from the Table 3 the amplitude of variability is larger in V band LCs than the R passband LCs. The amplitude of variations is mostly found to increase with frequency thus implying that the source spectrum becomes flatter when brightness of source increases (Massaro et al. 1998) which is also the case with our target.

The average spectral indices quoted in Table 4 are calculated simply as (Wierzcholska et al. 2015),

$$\langle \alpha_{VR} \rangle = \frac{0.4 \langle V - R \rangle}{\log(\nu_V / \nu_R)}, \quad (8)$$

where ν_V and ν_R are effective frequencies of the respective bands (Bessell, Castelli, & Plez 1998). The optical continuum of the source was very steep on most of the nights with $\alpha_{VR} > 3.8$ indicating strong synchrotron emission from the blazar jet and very less accretion disc contribution. Variation of spectral index with time is shown in Figure 5 giving the average spectral index during the entire observation cycle as ~ 4.2 .

The STV LC for the target during full monitoring period is displayed in Figure 1. The short term variability amplitude between JD 2456955.5 and JD 2456984.5 was found to increase with frequency i.e followed the same trend as was found on intra-night basis with values in B band $\sim 81.28\%$, V band $\sim 74.40\%$, R band $\sim 59.90\%$ and I band $\sim 59.70\%$, respectively, calculated using equation (4) above. We have also investigated the corresponding variations in (V-R) colour indices on intraday basis using the analysis criterion

described above and found that the BL Lacertae showed hints of colour variations on 2 of the nights i.e., on 26 and 27 Oct 2014 with maximum amplitude of variability reaching 6.94% on 27 Oct. Behaviour of (V-R) and (B-I) with time as shown in Figure 1 top panel indicates that colour variation is indeed variable on short term basis. The maximum (V-R) colour variation in the source on short timescale was of 0.838 (between its colour index of 0.826 on JD 2456955.5 and of 0.681 on JD 2456984.5) while for (B-I) maximum colour variation is found to be 2.726 (between 2.676 on JD 2456955.5 and 2.460 on the last day of our observation span i.e JD 2456984.5). We got large values of (B-I) as compared to (V-R) as is also evident from Figure 1, which is expected since the standard deviation is likely to increase with frequency separation between two bands.

5 INTRA- AND INTER-BAND CORRELATIONS

To search for the presence of any characteristic timescale of variability we performed the auto-correlation function (ACF) technique discussed in above sections by auto-correlating the R band which gives the ACF value of ~ 1 with nearly zero time lag and then dropping to negative values on most of the nights. From this we inferred that the LCs in R band are auto correlated with themselves and any characteristic variability timescale is absent.

From the intraday LCs in Figure 2, we infer the variations to be simultaneous in both the filters which was confirmed by DCF analysis technique as explained in section 3.2 with DCF bin sizes from 1 to 10 minutes. We are getting a strong peak (with DCF ~ 1) at time lag of 0 hrs to 0.007 hrs as clear from the Figure 3. These time lag values cannot be considered significant since they are close to the measurement intervals. The small frequency intervals in the optical regime leading to null time lags implies that the photons in these wavebands are emitting by same physical process and from the same emitting region. A significant positive lag in V vs R band DCF plots would imply that the V band variations lead those of the R filter. The V band magnitude vs R band magnitude plots in Figure 4 also clearly depicts that the flux variations are well correlated on almost all nights including those when the source was found to be variable indicating that the variability mechanism seems to be same in both the passbands. A linear model of the form $Y = mX + c$ was used to fit these plots whose results are given in Table 4 confirming that LCs in both the bands are closely correlated on all those nights when genuine variability was detected.

6 COLOUR-MAGNITUDE RELATIONSHIP

We then studied the behaviour of the spectral variations with respect to the brightness in V band for our source. We fitted straight lines ($CI = mV + c$) on each plot of colour index, CI, against V magnitude and fitted values for the slope, m_2 , along with constant, c_2 , are listed in Table 5. Significant positive correlation (the null hypothesis probability, $p \leq 0.05$) between colour index and apparent blazar magnitude indicates that the source exhibits a bluer when brighter or redder when fainter trend (H.E.S.S. Collaboration et al. 2014). In the following analysis, the observed magnitudes have been corrected for galactic extinction based on the extinction map of Schlegel et al. (1998) using NED extinction calculator ($A_V = 0.901$ mag, $A_R = 0.713$ mag). The flux from the nucleus of BL Lacertae is contaminated by the emissions of its giant elliptical host

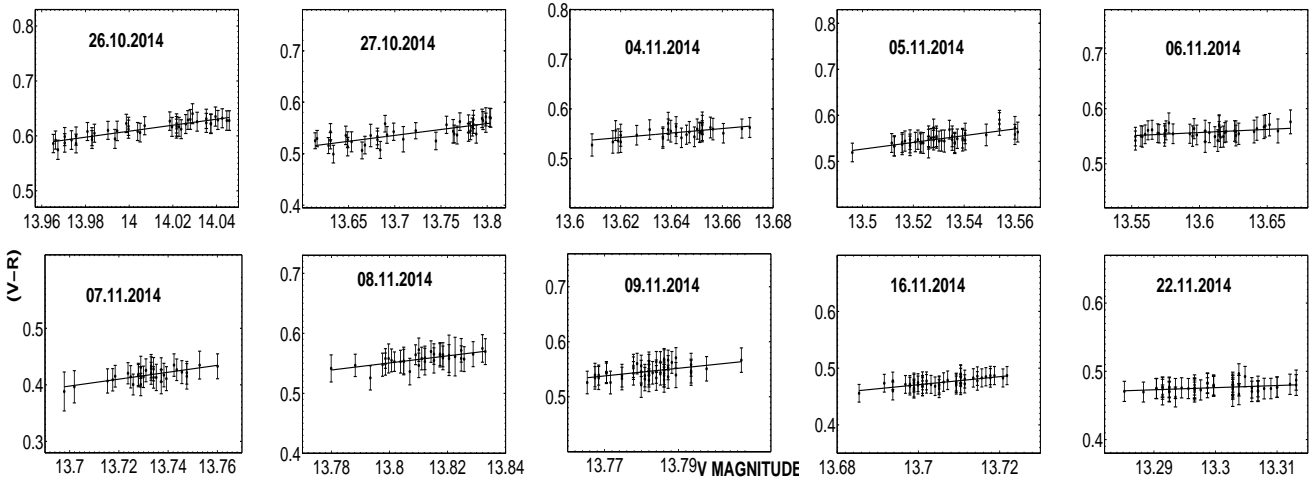


Figure 6. Colour magnitude plots on intraday timescales for BL Lacertae. The V magnitudes are given on the X-axis and the (V-R) colour index is plotted against them for each labeled date of observation.

galaxy. So the data is also corrected for the host galaxy contribution, using the measurements of Nilsson et al. (2007) to estimate the host galaxy emission in the R band which is then used to find the corresponding contributions for the V band (Fukugita et al. 1995; Gaur, Gupta, & Wiita 2012). During our observations we found that BWB trend was dominant for the source on intra-night timescales since we are getting significant positive correlation ($p \leq 0.05$) between the V magnitude and (V-R) colour index. We calculated the slope, m_2 , and the constant, c_2 , along with linear Pearson correlation coefficients and the corresponding null hypothesis probability, p_2 from the colour-magnitude plots (V-R colour Vs V magnitude) for the target for each night, as presented in Figure 6. On short term basis also we found that (V-R) colour indices follow the BWB trend indicating hardening of the spectrum as the source brightens with values of $m_3 = 0.1369 \pm 0.001$, $c_3 = -1.2602 \pm 0.01$, $r_3 = 0.4925 \pm 0.002$, and $p_3 = 0.0000$. We need dense, high precision data to clearly know about the trend in short term colour behaviour of the BL Lacertae.

Clear global BWB trend was observed in all 10 nights on intraday timescales with correlation coefficient ranging between 0.4 and 0.9. The source brightness was found to have strong BWB chromatism on intraday timescales. The BWB trend has been found to be predominant in BL Lacertae by all optical observations of this source till date during both flaring and steady states (Ghosh et al. 2000; Gaur et al. 2012; Gu et al. 2006) which was revealed by our observations also. Villata et al. (2004b) found that the intraday flares followed BWB trend strongly with a slope of ~ 0.4 which is also the case for our data with the slopes of the intra-night LCs more than ~ 0.4 in majority of cases. Thus, our colour variability results for the source being strongly chromatic between Oct - Nov 2014 were consistent with those of Villata et al. (2004b). Since the jet emissions are completely dominating the flux from BL Lacertae objects, this can be explained by the shock-in-jet models elaborated under section 8.

7 SPECTRAL ENERGY DISTRIBUTION (SED)

Differences in the physical parameters of the relativistic jet causes spectral changes in the emitting electrons which is the reason for SED changes thus rendering SED studies very useful. It will not

only help in understanding the emitting region but also help in discriminating between models and put tight constraints on those model parameters that are likely to change.

The low energy component of the blazar SED is commonly attributed to the synchrotron process in the relativistic jets while the Compton up-scattering of the low energy photons is probably the source of high energy component (e.g., Padovani & Giomini 1995; Sikora & Madejski 2001; Coppi 1999). These external photons could be originating from the Accretion Disc by thermal radiation, molecular torus, reprocessed disc emission from the broad line region (BLR) or from the hot corona (Sikora et al. 1994; Dermer & Schlickeiser 1993). The accretion disc luminosity along with the distance of the emitting region from the super massive black hole (SMBH) decides the intensity of each external photon. High energy emission is still not fully understood but for better understanding the proposed theoretical scenarios fall under two categories i.e the leptonic and the hadronic models. Leptonic models describe the gamma-ray emission produced by IC scattering of photons off the relativistic electrons while the hadronic models accounts for acceleration of protons in the relativistic Doppler boosted jet to energies sufficient for photo-pion production which further leads to pion decay and associated particle cascades (Celotti & Ghisellini 2008; Böttcher et al. 2007).

In this section, we focus on understanding SED changes associated with the target corresponding to the observed changes in their respective optical fluxes. In blazars, optical brightness changes is linked to changes in the spectral shapes and can be quantified by studying the properties of colour indices. The calibrated magnitudes of BL Lacertae were de-reddened by subtracting Galactic absorption $A_B = 1.192$ mag, $A_V = 0.901$ mag, $A_R = 0.713$ mag, and $A_I = 0.495$ mag (Cardelli et al. 1989; Bessell et al. 1998). Figure 7 shows optical SED for the source, generated using our B, V, R, I data sets for 13 different epochs with different flux levels. The faintest SED for BL Lacertae was measured on 2014 Oct 26. Significant variations were seen in the SEDs during Oct - Nov when it increased in brightness day by day, reaching a maximum on Nov 22. The synchrotron peak frequency has values between 10^{13} Hz and 10^{17} Hz. Since the optical band for this source lie near the peak of the synchrotron component of the SED, the optical variability reflects acceleration processes acting on the highest

Table 4. Results of linear fit to R Vs V plots and average spectral index values.

Observation Date	m_1^a	c_1^a	r_1^a	p_1^a	$\langle\alpha_{VR}\rangle$
26.10.2014	0.454 ± 0.006	7.309 ± 0.081	0.862 ± 0.008	<0.0001	4.605 ± 0.034
27.10.2014	0.769 ± 0.004	2.630 ± 0.060	0.971 ± 0.002	<0.0001	4.206 ± 0.038
04.11.2014	0.548 ± 0.016	5.805 ± 0.228	0.703 ± 0.021	<0.0001	4.272 ± 0.046
05.11.2014	0.267 ± 0.013	9.801 ± 0.183	0.388 ± 0.022	0.0101	4.252 ± 0.050
06.11.2014	0.885 ± 0.005	0.913 ± 0.073	0.965 ± 0.002	<0.0001	4.297 ± 0.042
07.11.2014	0.387 ± 0.017	8.324 ± 0.252	0.522 ± 0.027	0.0022	3.540 ± 0.047
08.11.2014	0.411 ± 0.015	7.890 ± 0.218	0.566 ± 0.024	0.0004	4.301 ± 0.045
09.11.2014	0.302 ± 0.024	9.475 ± 0.348	0.221 ± 0.011	0.1310	4.240 ± 0.045
16.11.2014	0.290 ± 0.012	9.662 ± 0.176	0.409 ± 0.020	0.0048	3.855 ± 0.033
22.11.2014	0.686 ± 0.014	3.768 ± 0.194	0.644 ± 0.014	<0.0001	3.852 ± 0.030

^a m_1 = slope and c_1 = intercept of CI against V;
 r_1 = Pearson coefficient; p_1 = null hypothesis probability

energy electrons. Due to the lack of multi-wavelength data here, a detailed description is bit difficult.

8 DISCUSSION AND CONCLUSION

To explain optical IDV several theoretical models have been proposed by authors which are broadly classified as extrinsic and intrinsic. The intrinsic origin of variability in blazars is either due to accretion disc instabilities or relativistic jet activities and is seen at all accessible timescales ranging from a few tens of minutes through days and months to even decades. Extrinsic mechanisms include interstellar scintillation causing radio variations (e.g. Heeschen et al. 1987) at low frequencies and can therefore not be the case of optical intra-night optical variability (INOV). Small variations can be explained by turbulence behind an outgoing shock along the jet. For high SMBH masses (most likely in excess of $10^8 M_\odot$) the light crossing time is very large which can be linked with this shortest variability timescales. Among the several accepted theoretical models explaining variability in BL Lacerate objects is the one involving shocks propagating down the inhomogeneous medium in the relativistic jets. The short timescale variations which we are concerned with like IDV and STV can be attributed to the irregularities in the jets caused due to the outgoing shocks and high optical polarization (Gaur et al. 2014) in case of BL Lacerate objects. The observed radiation from our source is predominantly non thermal Doppler boosted jet emission (Marscher & Gear 1985) thus reducing the observed variability timescale with respect to the rest frame timescale by Doppler factor δ , while increased by $(1+z)$ where z is the redshift. Spectrum steepening as magnitude increases can explain the presence of two components, one variable (with a flatter slope, α_1) ($f_\nu \propto \nu^{-\alpha}$) and the other one stable (with $\alpha_{const} > \alpha_1$), contributing to the overall optical emission. When the variable component dominates we get a chromatic behaviours. Villata et al. (2004a) confirmed that the optical variations on short timescales can be interpreted due to strongly chromatic component while the longer timescale component as mildly chromatic component. The BWB trend could be explained by one component synchrotron model which tells that more intense the energy release, the higher the particular frequency (Fiorucci, Ciprini, & Tostiet al. 2004) or due to the Doppler factor variations in a spectrum deviating from power law. It may be due to the intrinsic processes related to jet emission mechanism. Luminosity increase due to injection of fresh electrons with the energy distribution harder

than that of the previously cooled ones can also cause flattening of spectrum as the object brightens (Mastichiadis & Kirk 2002). According to the shock-in-jet model, as the shock propagating down the jet strikes a region of high electron population, radiations at different visible colours is produced at different distances behind the shocks. High energy photons from synchrotron mechanism typically emerge sooner and closer to the shock front than the lower frequency radiation thus causing colour variations. The BWB situation obtained in this paper will be dominant during the rising phase of a flare which is most common in case of BL Lacerate objects as they are beamed but intrinsically weak thus causing the observed optical emission from BL Lacerate objects to be overwhelmed by that from the relativistic jets. Hawkins (2002) said that the effect of the underlying host galaxy and the colour changes from microlensing can also lead to colour variations with time. But since in BL Lacerate objects the Doppler boosting flux from the relativistic jet almost invariably swamps the light from the host galaxy, the galaxy's light contribution in the observed emission is very less especially during the flaring states, thereby making the red shift determination very difficult. Latest studies of Sun et al. (2014) discovered a timescale dependent colour variations. They said that the colour of the variable emission is timescale independent thus ruling out the possibility of BWB trend being due to the contamination from a non-variable redder component, such as host galaxy. The model states that for timescales < 30 days, the BWB trend in quasars is even stronger and it gradually weakens with the increasing timescales of above 100 days. Gravitational microlensing is important on weeks to months timescales and is achromatic, so flux and colour variations observed by us on intraday timescale can be most likely explained by the jet based models explained above. Since jets in BL Lacerate objects are pointed between $6^\circ - 10^\circ$ with the LOS of the observer, the radiation from it, especially in active phase is dominated by emissions from the relativistic jets while disc emission is much weaker, hence the jet models can explain the flux and colour variability detected by us. Doppler boosting greatly amplifies even very weak flux variations produced due to small changes in the magnetic field or electron density. There are several possibilities causing SED changes including freshly injected electrons with energy distribution higher than the average causing higher synchrotron emission and a peak blue shifting or another reason could be of change in the Doppler boosting factor presumably due to change in the viewing angle. The changes in the magnetic field can also lead to variations in the SED of BL Lac-

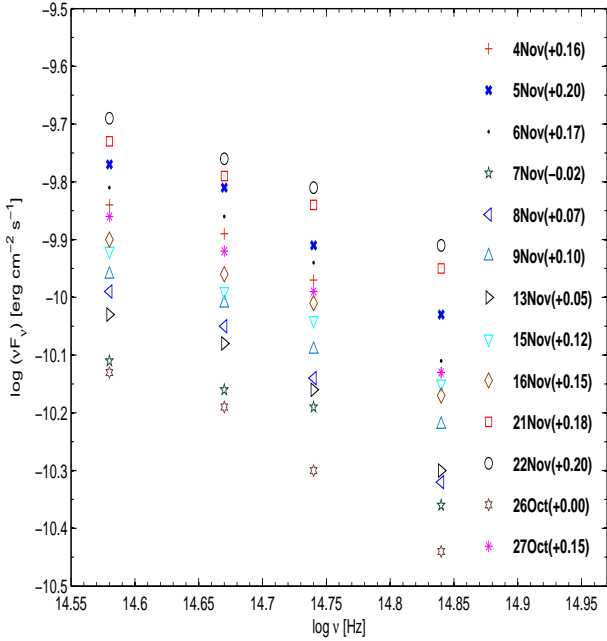


Figure 7. SED results for BL Lacertae in optical frequencies. Different symbols are used for each epoch mentioned in the figure along with the offset used.

erate objects. To explore above mentioned reasons in greater detail we would require data covering the entire EM spectra.

In this paper, we carried out multi-band optical photometry for BL Lacertae between 25 Oct - 23 Nov 2014, in a total of 13 nights, in B, V, R, and I passbands. Among these 13 nights are 10 dates on which we also carried out quasi-simultaneous observations in V and R filters (as mentioned in Table 2). We found that the source showed displayed genuine IDV on 3 nights in both V and R bands. If we include PV cases as well then confirmed microvariability was found on 9 out of 10 nights in R passband while on 5 nights in V filter. Variability results can be improved by lengthier observations. Chances of getting variability on intranight timescales are maximum when a blazar is observed for 6–7 hrs as was said by Carini et al. (2007) where authors also found that less than 10% of the sources under study revealed IDV when observed for ~ 4 –5 hrs which is the range for most of our observations also. In the cases where strong variability is found, its amplitude is greater in higher frequency bands which is consistent with Papadakis et al. (2003). We also carried out DCF analysis to search for the periodicity and any variability timescale but none was found to be present in any of the LCs which could be possible if the timescale of electron distribution evolution is longer than the typical monitoring time (i.e. longer than ~ 4 hrs) (Bachev et al. 2011). We also searched for correlation between colour and magnitude and found that our source follows BWB trend which help us to shed some light on the emission mechanism and emission region. The BL Lacertae objects are on the descending part of the first SED bump where optical spectral index (α) should be > 1 , which is also obtained for our source. BL Lacertae was found to have steep optical spectra with spectral index > 3.5 on all observation nights. We generated spectral energy distribution of the source using the B, V, R, and I data points for all 13 nights with magnitudes in all bands being de-reddened using

Table 5. Fits to colour-magnitude dependencies and colour-magnitude correlation coefficients.

Observation Date	m_2^a	c_2^a	r_2^a	p_2^a
26.10.2014	0.546 ± 0.006	-7.031 ± 0.077	0.898 ± 0.006	<0.0001
27.10.2014	0.229 ± 0.004	-2.608 ± 0.056	0.771 ± 0.013	<0.0001
04.11.2014	0.450 ± 0.016	-5.590 ± 0.214	0.630 ± 0.025	<0.0001
05.11.2014	0.733 ± 0.013	-9.368 ± 0.172	0.756 ± 0.013	<0.0001
06.11.2014	0.115 ± 0.005	-1.000 ± 0.069	0.431 ± 0.022	0.0049
07.11.2014	0.611 ± 0.017	-7.966 ± 0.239	0.693 ± 0.021	<0.0001
08.11.2014	0.589 ± 0.015	-7.577 ± 0.206	0.701 ± 0.019	<0.0001
09.11.2014	0.698 ± 0.024	-9.077 ± 0.328	0.464 ± 0.018	0.0009
16.11.2014	0.710 ± 0.012	-9.258 ± 0.167	0.731 ± 0.012	<0.0001
22.11.2014	0.312 ± 0.014	-3.670 ± 0.182	0.356 ± 0.019	0.0104

^a m_2 = slope and c_2 = intercept of CI against V;

r_2 = Pearson coefficient; p_2 = null hypothesis probability

the galactic extinction coefficient values. SED studies can provide some useful information about the possible physical causes of the observed spectral variability.

ACKNOWLEDGMENTS

We thank the referee for detailed and thoughtful comments which helped us to improve the manuscript.

REFERENCES

- Abdo A. A., et al., 2010, ApJ, 716, 30
- Bachev R., et al., 2011, A&A, 528, LL10
- Bessell M. S., Castelli F., Plez B., 1998, A&A, 333, 231
- Blandford R. D., Rees M. J., 1978, PhysS, 17, 265
- Böttcher M., et al., 2003, ApJ, 596, 847
- Böttcher M., et al., 2007, ApJ, 670, 968
- Cardelli J. A., Clayton G. C., Mathis J. S., 1989, ApJ, 345, 245
- Carini M. T., Miller H. R., Noble J. C., Goodrich B. D., 1992, AJ, 104, 15
- Carini M. T., Noble J. C., Taylor R., Culler R., 2007, AJ, 133, 303
- Celotti A., Ghisellini G., 2008, MNRAS, 385, 283
- Clements S. D., Carini M. T., 2001, AJ, 121, 90
- Coppi P. S., Aharonian F. A., 1999, ApJ, 521, L33
- de Diego J. A., 2010, AJ, 139, 1269
- Dermer C. D., Schlickeiser R., 1993, ICRC, 1, 160
- Edelson R. A., Krolik J. H., 1988, ApJ, 333, 646
- Fan J. H., Lin R. G., 2000, ApJ, 537, 101
- Fiorucci M., Ciprini S., Tosti G., 2004, A&A, 419, 25
- Fossati G., Celotti A., Ghisellini G., Maraschi L., 1997, MNRAS, 289, 136
- Fossati G., Maraschi L., Celotti A., Comastri A., Ghisellini G., 1998, MNRAS, 299, 433
- Fukugita M., Shimasaku K., Ichikawa T., 1995, PASP, 107, 945
- Gaur H., et al., 2012, MNRAS, 420, 3147
- Gaur H., Gupta A. C., Wiita P. J., 2012, AJ, 143, 23
- Gaur H., Gupta A. C., Wiita P. J., Uemura M., Itoh R., Sasada M., 2014, ApJ, 781, LL4
- Ghisellini G., et al., 1997, A&A, 327, 61
- Ghosh K. K., Ramsey B. D., Sadun A. C., Soundararajaperumal S., Wang J., 2000, ApJ, 537, 638

- Gopal-Krishna, Stalin C. S., Sagar R., Wiita P. J., 2003, *ApJ*, 586, L25
- Gu M. F., Lee C.-U., Pak S., Yim H. S., Fletcher A. B., 2006, *A&A*, 450, 39
- Gupta A. C., Banerjee D. P. K., Ashok N. M., Joshi U. C., 2004, *A&A*, 422, 505
- Gupta A. C., Fan J. H., Bai J. M., Wagner S. J., 2008, *AJ*, 135, 1384
- Hawkins M. R. S., 2002, *ASPC*, 284, 351
- Heeschen D. S., Krichbaum T., Schalinski C. J., Witzel A., 1987, *AJ*, 94, 1493
- Heidt J., Wagner S. J., 1996, *A&A*, 305, 42
- H.E.S.S. Collaboration, et al., 2011, *A&A*, 533, AA110
- H.E.S.S. Collaboration, et al., 2014, *A&A*, 571, AA39
- Hovatta T., Tornikoski M., Lainela M., Lehto H. J., Valtaoja E., Tornainen I., Aller M. F., Aller H. D., 2007, *A&A*, 469, 899
- Jang M., Miller H. R., 1997, *AJ*, 114, 565
- Marscher A. P., Gear W. K., 1985, *ApJ*, 298, 114
- Mastichiadis A., Kirk J. G., 2002, *PASA*, 19, 138
- Massaro E., Nesci R., Maesano M., Montagni F., D'Alessio F., 1998, *MNRAS*, 299, 47
- Miller J. S., Hawley S. A., 1977, *ApJ*, 212, L47
- Mukherjee R., et al., 1997, *ApJ*, 490, 116
- Nieppola E., Tornikoski M., Valtaoja E., 2006, *A&A*, 445, 441
- Nilsson K., Pasanen M., Takalo L. O., Lindfors E., Berdyugin A., Ciprini S., Pforr J., 2007, *A&A*, 475, 199
- Padovani P., Giommi P., 1995, *MNRAS*, 277, 1477
- Padovani P., Giommi P., 1996, *MNRAS*, 279, 526
- Papadakis I. E., Boumis P., Samaritakis V., Papamastorakis J., 2003, *A&A*, 397, 565
- Raiteri C. M., et al., 2009, *A&A*, 507, 769
- Raiteri C. M., et al., 2013, *MNRAS*, 436, 1530
- Rani B., Wiita P. J., Gupta A. C., 2009, *ApJ*, 696, 2170
- Ravasio M., et al., 2002, *A&A*, 383, 763
- Rector T. A., Perlman E. S., 2003, *AJ*, 126, 47
- Romero G. E., Cellone S. A., Combi J. A., 1999, *A&AS*, 135, 477
- Sambruna R. M., Maraschi L., Urry C. M., 1996, *ApJ*, 463, 444
- Schlegel D. J., Finkbeiner D. P., Davis M., 1998, *ApJ*, 500, 525
- Schmitt J. L., 1968, *Natur*, 218, 663
- Sikora M., Madejski G., 2001, *AIPC*, 558, 275
- Stalin C. S., Gopal-Krishna, Sagar R., Wiita P. J., 2004, *MNRAS*, 350, 175
- Stetson P. B., 1987, *PASP*, 99, 191
- Stetson P. B., 1992, *ASPC*, 25, 297
- Stoeck J. T., Liebert J., Schmidt G., Gioia I. M., Maccacaro T., Schild R. E., Maccagni D., Arp H. C., 1985, *ApJ*, 298, 619
- Stoeck J. T., Morris S. L., Gioia I. M., Maccacaro T., Schild R. E., Wolter A., 1989, *LNP*, 334, 242
- Sun Y.-H., Wang J.-X., Chen X.-Y., Zheng Z.-Y., 2014, *ApJ*, 792, 54
- Urry C. M., Padovani P., 1995, *PASP*, 107, 803
- Villata M., et al., 2002, *A&A*, 390, 407
- Villata M., et al., 2004a, *A&A*, 424, 497
- Villata M., et al., 2004b, *A&A*, 421, 103
- Wagner S. J., Witzel A., 1995, *ARA&A*, 33, 163
- Weeks J. R., 2003, *MPLA*, 18, 2099
- Wierzcholska A., Ostrowski M., Stawarz Ł., Wagner S., Hauser M., 2015, *A&A*, 573, AA69
- Wurtz R., Stoeck J. T., Yee H. K. C., 1996, *ApJS*, 103, 109